

1-11-2017

Epitaxial strain controlled magnetocrystalline anisotropy in ultrathin FeRh/MgO bilayers

Guohul Zheng

Tongji University & California State University

San-Huang Ke

Tongji University, shke@tongji.edu.cn

Maosheng Miao

California State University

Jinwoong Kim


California State University

R, Ramesh

Lawrence Berkeley National Laboratory

See next page for additional authors

Follow this and additional works at: <http://digitalcommons.unl.edu/cmrafacpub>

 Part of the [Atomic, Molecular and Optical Physics Commons](#), [Condensed Matter Physics Commons](#), [Engineering Physics Commons](#), and the [Other Physics Commons](#)

Zheng, Guohul; Ke, San-Huang; Miao, Maosheng; Kim, Jinwoong; Ramesh, R., and Kioussis, Nicholas, "Epitaxial strain controlled magnetocrystalline anisotropy in ultrathin FeRh/MgO bilayers" (2017). *Faculty Publications from Nebraska Center for Materials and Nanoscience*. 124.

<http://digitalcommons.unl.edu/cmrafacpub/124>

This Article is brought to you for free and open access by the Materials and Nanoscience, Nebraska Center for (NCMN) at DigitalCommons@University of Nebraska - Lincoln. It has been accepted for inclusion in Faculty Publications from Nebraska Center for Materials and Nanoscience by an authorized administrator of DigitalCommons@University of Nebraska - Lincoln.

Authors

Guohul Zheng; San-Huang Ke; Maosheng Miao; Jinwoong Kim; R, Ramesh; and Nicholas Kioussis

Epitaxial strain controlled magnetocrystalline anisotropy in ultrathin FeRh/MgO bilayers

Guohui Zheng,^{1,2} San-Huang Ke,^{1,a} Maosheng Miao,³ Jinwoong Kim,² R. Ramesh,⁴ and Nicholas Kioussis^{2,b}

¹MOE Key Laboratory of Microstructured Materials, School of Physics Science and Engineering, Tongji University, 1239 Siping Road, Shanghai 200092, China

²Department of Physics, California State University, Northridge, California 91330-8268, USA

³Department of Chemistry and Biochemistry, California State University, Northridge, California 91330-8268, USA

⁴Materials Sciences Division, Lawrence Berkeley National Laboratory, Berkeley, California 94720, USA

(Presented 3 November 2016; received 22 September 2016; accepted 25 October 2016; published online 11 January 2017)

Using *ab initio* electronic structure calculations we have investigated the effect of epitaxial strain on the magnetocrystalline anisotropy (MCA) of ultrathin FeRh/MgO heterostructures. Analysis of the energy- and k-resolved distribution of the orbital character of the band structure reveals that MCA largely arises from the spin-orbit coupling (SOC) between $d_{x^2-y^2}$ and d_{xz}/d_{yz} orbitals of Fe atoms at the FeRh/MgO interface. We demonstrate that the strain has significant effects on the MCA: It not only affects the value of the MCA but also induces a switching of the magnetic easy axis from perpendicular to in-plane direction. The mechanism is the strain-induced shifts of the SOC *d*-states. Our work demonstrates that strain engineering can open a viable pathway towards tailoring magnetic properties for antiferromagnetic spintronic applications. © 2017 Author(s). All article content, except where otherwise noted, is licensed under a Creative Commons Attribution (CC BY) license (<http://creativecommons.org/licenses/by/4.0/>). [<http://dx.doi.org/10.1063/1.4974059>]

I. INTRODUCTION

The field of antiferromagnetic (AFM) spintronics^{1,2} is attracting increasing attention in the materials science community. With device structures being similar to their ferromagnetic (FM) counterparts, AFM spintronics complements or replaces ferromagnets by antiferromagnets in the active components of spintronic devices. Owing to the staggered magnetic order, antiferromagnets are insensitive to disturbing magnetic fields and do not produce stray fields. Moreover, the intrinsic high frequencies of AFM dynamics^{2,3} also make them distinct from ferromagnets. Due to these prominent properties, antiferromagnets have been used as magnetic recording media^{4-6,9} with good performance. Among various AFM materials the near equiatomic chemically ordered bcc-B2 (CsCl-type) bulk FeRh alloy is attracting intense interest due to its unusual first-order phase transition from AFM to FM order at ~ 350 K. This is accompanied with a volume expansion of ~ 1% indicating a coupling between the spin and structural degrees of freedom.^{7,8} Together with the relativistic effects present in FeRh (such as magnetocrystalline anisotropy, MCA), thermally assisted FeRh-based memory have been successfully fabricated.⁹ Most of density functional theory calculations¹⁰⁻¹² to date have focused on the electronic structure properties solely of the bulk bcc structure under hydrostatic pressure. On the other hand, FeRh thin films are grown epitaxially on MgO,¹³ BaTiO₃,^{14,15} or piezoelectric¹⁶ substrates, where the lattice mismatch inevitably generates strain which may modulate the magnetic properties of the FeRh overlayer. Recent *ab initio* electronic structure calculations have investigated

^aE-mail: shke@tongji.edu.cn.

^bE-mail: nick.kioussis@csun.edu.

the relative stability of the FM, “bcc-like-AFM”, and “fcc-like-AFM” structures under epitaxial strain.¹⁷ Therefore, it is of great importance to understand the effect of strain on the MCA of ultrathin FeRh thin films for further promoting their applications in AFM spintronics.

In this work, we investigate the effect of epitaxial strain on the MCA of FeRh/MgO ultrathin heterostructure by performing *ab initio* density functional theory (DFT) electronic structure calculations. We find that the value of MCA and the direction of magnetic easy axis strongly depend on the strain leading to a spin re-orientation from an in- to out-of-plane magnetization orientation in the AFM phase and across the metamagnetic transition. The underlying mechanism is explained by analyzing the band structure and the strain-induced shifts of distribution of orbital characters. Our work demonstrates that strain engineering can serve as a viable and efficient approach in tuning the magnetization directions in FeRh.

II. COMPUTATIONAL DETAILS

We use the Vienna *ab initio* simulation package (VASP)^{19–21} to perform the electronic structure calculations. The projector augmented wave formalism¹⁸ is adopted for describing the electron-ion interactions, and plane waves with a kinetic energy cutoff of 500 eV are used to expand the wave functions. The generalized gradient approximation (GGA) in the version of Perdew-Burke-Ernzerhof (PBE)²² is adopted for treating the electron exchange and correlation. The GGA exchange correlation functional has been shown to provide a reasonable description of the structural properties of FeRh, in contrast to the local density approximation which yields incorrectly that the fcc-like AFM phase is the ground state.¹⁷ With a Monkhorst-Pack k -mesh of $31 \times 31 \times 31$ for Brillouin zone (BZ) sampling, the calculated equilibrium lattice constants (a) of bulk G-AFM and FM phase FeRh are 2.995 Å and 3.012 Å, respectively, in good agreement with available experimental data.⁸

The ultrathin FeRh (001) film on the rock-salt MgO (001) substrate is modeled by a slab structure, as is shown in Fig. 1. The slab supercell consists of five monolayers (ML) of FeRh with each ML consisting of two Fe or Rh atoms, which are placed on the top of a MgO slab. A 12-Å thick vacuum region is introduced in the supercell to avoid the artificial interactions between the slab and its images created by the periodic boundary conditions. The $\langle 110 \rangle$ axis of FeRh is aligned with the $\langle 100 \rangle$ axis of MgO and the O atoms at the FeRh/MgO interface are placed atop of the Fe atoms. In this work we consider the Fe-terminated interface and surface in both the G-AFM and FM phases, respectively.

We consider three different in-plane lattice constants for the MgO substrate: the equilibrium one of the G-AFM phase $\sqrt{2} \times 2.995 = 4.236$ Å, the equilibrium one of the FM phase $\sqrt{2} \times 3.012 = 4.260$ Å, and the equilibrium one of the MgO 4.212 Å. The lattice constant mismatch between the FeRh film and MgO substrate will create a biaxial strain in the FeRh film, which may play an important role on the MCA of the bilayer system. Here, the strain is defined with respect to the equilibrium lattice of G-AFM phase, $\eta = (a_{\text{FeRh}} - a_{\text{G-AFM FeRh}}) / a_{\text{G-AFM FeRh}} \times 100\%$. Therefore, for the three in-plane lattice constants considered, the strains are -0.57 %, 0 %, and 0.57 %, respectively.

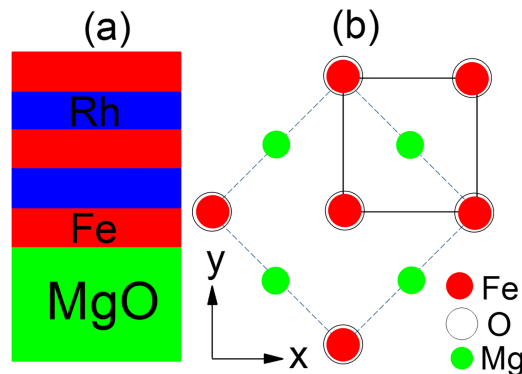


FIG. 1. (a) Illustration of the Fe terminated FeRh/MgO heterostructure, (b) atomic configuration at the FeRh/MgO interface, where the O atoms are placed atop of the Fe atoms.

For each strain condition, the magnetic and electronic degrees of freedom and the atomic z positions are fully relaxed until the maximum force acting on each single ion is less than 0.01 eV/\AA . A Monkhorst-Pack k -mesh of $15 \times 15 \times 1$ is used in the selfconsistent DFT calculations followed by a $31 \times 31 \times 1$ k -mesh for the scalar relativistic calculations with the spin-orbit coupling (SOC). The MCA per interfacial area is determined by $[E_{[100]} - E_{[001]}]/A$, where $E_{[100]}$ ($E_{[001]}$) is the total energy with SOC included along the $[100]$ and $[001]$ directions, respectively.

III. RESULTS AND DISCUSSION

In Table I we list the calculated values of the strain dependence of the spin magnetic moments (m_s), orbital magnetic moment differences (Δm_o) of the interfacial Fe atom (Fe_i) and surface Fe atom (Fe_s), respectively, for both the G-AFM and FM phases, respectively. We also list the MCA values and the total energy difference (ΔE) between the G-AFM and FM phases under different strain. Note because the two Fe atoms on each atomic plane in the G-AFM phase have opposite m_s , we only list its magnitude. We find that for the range of strain considered here the G-AFM phase is more stable than the FM phase, where the energy difference $\Delta E = E_{FM} - E_{G-AFM} \approx 20 \text{ meV/Fe}$ regardless of the strain. Previous DFT calculations^{26,27} for *free-standing* FeRh films reported values of $\sim 25 \text{ meV/Fe}$, indicating that the MgO substrate slightly decreases the energy difference between the two phases. The m_s values of Fe_i and Fe_s in the G-AFM and FM systems range from 3.02 to $3.19 \mu_B$, which are close to the bulk value of $\sim 3.1 \mu_B$, and depend weakly on strain. For the G-AFM phase the variation of MCA with strain is large and correlates well with the strain variation of Δm_o of Fe_i but not with that of Fe_s . For the G-AFM phase the compressive strain yields an in-plane magnetic easy axis while tensile strain induces an out-of-plane easy axis, where the spin reorientation occurs around $\eta \approx 0$. This strain induced MCA energy behavior is similar (opposite) to that in CoFe_2O_4 (CoCr_2O_4).²³ Furthermore, tensile strain induces an in-plane (out-of-plane) magnetic easy axis in Ta/FeCo/MgO (Au/FeCo/MgO) trilayers.^{24,25} Interestingly we find a spin-reorientation across the metamagnetic transition for $\eta = 0, -0.57\%$.

To understand the underlying mechanism of the strain effect, we plot in Fig. 2 the energy- and k -resolved distribution of the orbital character of the minority-spin bands of the spin-up interfacial iron Fe_i -derived $d_{xz,yz}$ and $d_{x^2-y^2}$ states for $\eta = -0.57\%$. (The analysis of the spin-down Fe_i atom is identical.) Within the second-order perturbation theory, the MCA can be expressed as:²⁸

$$\text{MCA} \propto \xi^2 \sum_{o,u} \frac{|\langle \Psi_o^\downarrow | \hat{L}_z | \Psi_u^\downarrow \rangle|^2 - |\langle \Psi_o^\downarrow | \hat{L}_{x/y} | \Psi_u^\downarrow \rangle|^2}{E_u^\downarrow - E_o^\downarrow} + \text{majority-spin term} + \text{spin-flip term}, \quad (1)$$

where the coupling matrix element $\langle \cdot | \cdot | \cdot \rangle$ denotes the SOC of the occupied state (Ψ_o) with eigenenergy E_o and the unoccupied state (Ψ_u) with eigenenergy E_u through angular momentum operator $\hat{L}_{x/y}$ or \hat{L}_z (contributes positively) with proper selection rules. Since our analysis for the spin-up Fe_i is in terms of the minority-spin bands, only the first term in Eq. (1) is important, because the majority spin bands are well below the Fermi energy.

TABLE I. Strain dependence of the spin magnetic moment (m_s) and orbital magnetic moment difference ($\Delta m_o = m_o^{[001]} - m_o^{[100]}$) along the $[001]$ and $[100]$ directions, of the interfacial (Fe_i) and surface (Fe_s) Fe atoms, for the AFM and FM phases, respectively. We list also the strain dependence of the MCA values of the G-AFM and FM FeRh/MgO bilayer, as well as the total energy difference between the two magnetic phases.

strain(%)	G-AFM					FM					$\Delta E = E_{FM} - E_{AFM}$ (meV/Fe)
	$m_s(\mu_B)$		$\Delta m_o(10^{-2}\mu_B)$		MCA	$m_s(\mu_B)$		$\Delta m_o(10^{-2}\mu_B)$		MCA	
	Fe_i	Fe_s	Fe_i	Fe_s	(erg/cm ²)	Fe_i	Fe_s	Fe_i	Fe_s	(erg/cm ²)	
-0.57	3.028	3.152	-3.6	-5.3	-0.47	3.068	3.180	5.9	2.3	0.45	19.3
0	3.027	3.153	-2.7	-5.7	-0.07	3.069	3.184	5.8	1.9	0.55	20.3
0.57	3.026	3.153	-1.7	-5.7	0.44	3.076	3.186	5.2	1.6	0.30	22.0

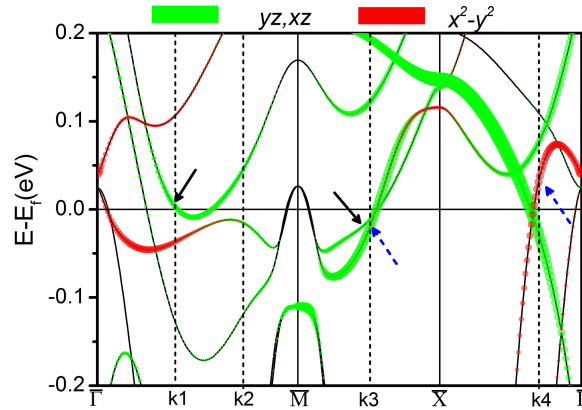


FIG. 2. Energy- and k -resolved distribution of orbital character of the minority-spin bands (under compressive strain of -0.57%) of the $d_{yz,xz}$ (green) and $d_{x^2-y^2}$ (red) orbitals of the spin-up interfacial Fe atom (Fe_i). \mathbf{k} points with large negative or positive contributions to the total MCA are indicated by $k1 - k4$ (based on the second-order perturbation theory of MCA). The bands prone to shift under different strains are indicated by arrows (black solid: up-shift, blue dashed: down-shift).

From Fig. 2 one can see that around the $k1$ and $k4$ points the unoccupied $d_{yz,xz}$ states couple to the occupied $d_{x^2-y^2}$ state through $\hat{L}_{x,y}$, giving negative contributions to the total MCA. On the other hand, in a wide region around $k2$ the occupied and unoccupied $d_{yz,xz}$ states couple through \hat{L}_z yielding large positive contributions. The sum over these \mathbf{k} points gives the negative MCA of -0.47 erg/cm^2 for $\eta = -0.57\%$. Note that around \mathbf{k} points $k1$, $k3$, and $k4$, few bands (indicated by the arrows in Fig. 2) cross the Fermi level and are prone to shift under different strain.

In Fig. 3 we show the minority-spin projected density of states (PDOS) of the spin-up Fe_i d_{yz} , d_{xz} , and $d_{x^2-y^2}$ orbitals for three strains. As one can see, with increasing η there is a redistribution of PDOS on $d_{x^2-y^2}$ from unoccupied to occupied, indicating a down-shift of this orbital across the Fermi level around $k4$. The PDOS distribution of d_{xz} orbital in the range of $[-0.2, 0.2]$ eV is slightly

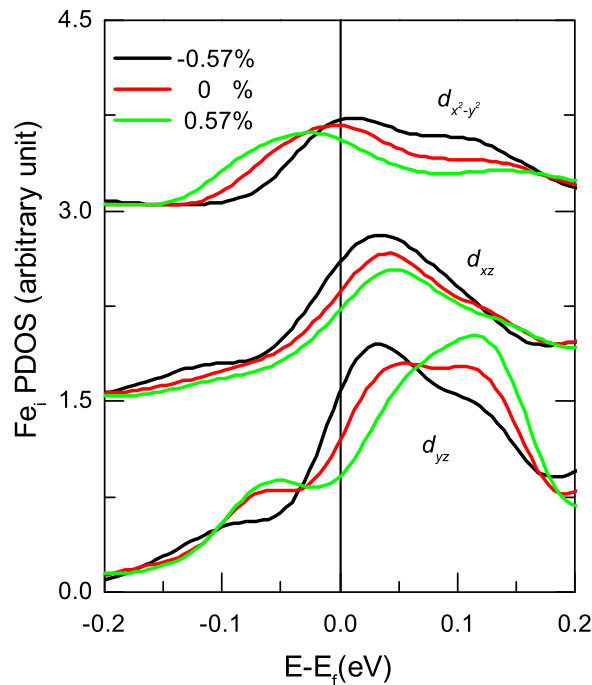


FIG. 3. Projected density of states (PDOS) (minority) on the spin-up Fe_i d_{yz} , d_{xz} , and $d_{x^2-y^2}$ orbitals for $\eta = -0.57, 0,$ and 0.57% , respectively. The PDOS of the d_{xz} and $d_{x^2-y^2}$ are shifted by 1.5 and 3 units along the vertical axis, respectively.

suppressed with increasing η . For d_{yz} orbital there are two large changes in its PDOS with increasing η : (i) The peak of unoccupied PDOS shifts from 0.025 to 0.15 eV, suggesting a upward-shift of this orbital around k1 and k3; (ii) The occupied PDOS distribution in the range of $[-0.1, -0.05]$ eV is largely enhanced due to the down-shift of the band indicated by the blue dashed arrow at k3. Overall, the band shifts will induce a large variation of MCA. Specifically, the band shifts around k1 and k4 decrease or disable the negative SOC while the band shifts at k3 enable the positive SOC. As a result, the MCA value changes from negative to positive when the strain changes from -0.57% to 0.57% .

IV. CONCLUSION

In summary, we have studied the effect of epitaxial strain on the MCA of an ultrathin FeRh/MgO bilayer system by performing *ab initio* DFT electronic structure calculations. Under a compressive strain of -0.57% , the system possesses a large MCA value with the magnetic easy axis being in-plane. Detailed analyses based on the perturbation theory show this is due to the $\langle d_{yz,xz} | \hat{L}_{x,y} | d_{x^2-y^2} \rangle$ coupling matrix elements. When the strain changes from compressive to tensile, the induced band shifts and the concomitant redistributions of PDOS greatly change the contribution from each \mathbf{k} point to the MCA, thus causing the reorientation of the magnetic easy axis from in- to out-of-plane. Our work demonstrates that strain engineering can be used to tailor the magnetic properties of AFM FeRh spintronic devices.

ACKNOWLEDGMENTS

This research was supported by NSF Grant No. ERC-Translational Applications of Nanoscale Multiferroic Systems (TANMS)-1160504, by NSF Grant No. DMR-1532249, and by the National Natural Science Foundation of China under Grant No. 11174220 and 11374226.

- ¹ T. Jungwirth, X. Marti, P. Wadley, and J. Wunderlich, *Nature Nanotech.* **11**, 231 (2016).
- ² E. V. Gomonay and V. Loktev, *Low Temp. Phys.* **40**, 17 (2014).
- ³ F. Keffer and C. Kittel, *Phys. Rev.* **85**, 329 (1952).
- ⁴ S. Loth, S. Baumann, C. P. Lutz, D. M. Eigler, and A. J. Heinrich, *Science* **335**, 196 (2012).
- ⁵ P. Wadley, B. Howells, T. Jungwirth *et al.*, *Science* **351**, 587 (2016).
- ⁶ A. V. Kimel, A. Kirilyuk, A. Tsvetkov, R. V. Pisarev, and T. Rasing, *Nature* **429**, 850 (2004).
- ⁷ J. S. Kouvel and C. C. Hartelius, *J. Appl. Phys.* **33**, 1343 (1962).
- ⁸ G. Shirane, C. W. Chen, P. A. Flinn, and R. Nathans, *Phys. Rev.* **131**, 183 (1963).
- ⁹ X. Marti, I. Fina, C. Frontera, J. Liu, P. Wadley, Q. He, R. J. Paull, J. D. Clarkson, J. Kudrnovský, I. Turek, J. Kuneš, D. Yi, J.-H. Chu, C. T. Nelson, L. You, E. Arenholz, S. Salahuddin, J. Fontcuberta, T. Jungwirth, and R. Ramesh, *Nat. Mater.* **13**, 367 (2014).
- ¹⁰ M. E. Gruner, E. Hoffmann, and P. Entel, *Phys. Rev. B* **67**, 064415 (2003).
- ¹¹ L. M. Sandratskii and P. Mavropoulos, *Phys. Rev. B* **83**, 174408 (2011).
- ¹² V. L. Moruzzi and P. M. Marcus, *Phys. Rev. B* **46**, 2864 (1992).
- ¹³ C. Bordel, J. Juraszek, D. W. Cooke, C. Baldasseroni, S. Mankovsky, J. Minár, H. Ebert, S. Moyerman, E. E. Fullerton, and F. Hellman, *Phys. Rev. Lett.* **109**, 117201 (2012).
- ¹⁴ R. O. Cherifi, V. Ivanovskaya, L. C. Phillips, A. Zobelli, I. C. Infante, E. Jacquet, V. Garcia, S. Fusil, P. R. Briddon, N. Guiblin, A. Mougin, A. A. Únal, F. Kronast, S. Valencia, B. Dkhil, A. Barthélémy, and M. Bibes, *Nat. Mater.* **13**, 345 (2014).
- ¹⁵ Z. Q. Liu, L. Li, Z. Gai, J. D. Clarkson, S. L. Hsu, A. T. Wong, L. S. Fan, M.-W. Lin, C. M. Rouleau, T. Z. Ward, H. N. Lee, A. S. Sefat, H. M. Christen, and R. Ramesh, *Phys. Rev. Lett.* **116**, 097203 (2016).
- ¹⁶ Y. Lee, Z. Q. Liu, J. T. Heron, J. D. Clarkson, J. Hong, C. Ko, M. D. Biegalski, U. Aschauer, S.-L. Hsu, M. E. Nowakowski, J. Wu, H. M. Christen, S. Salahuddin, J. B. Bokor, N. A. Spaldin, D. G. Schlom, and R. Ramesh, *Nat. Commun.* **6**, 5959 (2015).
- ¹⁷ U. Aschauer, R. Braddell, S. A. Brechbühl, P. M. Derlet, and N. A. Spaldin, *Phys. Rev. B* **94**, 014109 (2016).
- ¹⁸ P. E. Blöchl, *Phys. Rev. B* **50**, 17953 (1994).
- ¹⁹ G. Kresse and J. Furthmüller, *Phys. Rev. B* **54**, 11169 (1996).
- ²⁰ G. Kresse and J. Furthmüller, *Comput. Mater. Sci.* **6**, 15 (1996).
- ²¹ G. Kresse and D. Joubert, *Phys. Rev. B* **59**, 1758 (1999).
- ²² J. P. Perdew, K. Burke, and M. Ernzerhof, *Phys. Rev. Lett.* **77**, 3865 (1996).
- ²³ J. A. Heuver, A. Scaramucci, Y. Blickenstorfer, S. Matzen, N. A. Spaldin, C. Ederer, and B. Noheda, *Phys. Rev. B* **92**, 214429 (2015).
- ²⁴ P. V. Ong, N. Kioussis, D. Odkhuu, P. K. Amiri, K. L. Wang, and G. P. Carman, *Phys. Rev. B* **92**, 020407(R) (2015).
- ²⁵ P. V. Ong, N. Kioussis, P. K. Amiri, and K. L. Wang, *Scientific Reports* **6**, 29815 (2016).
- ²⁶ S. Lounis, M. Benakki, and C. Demangeat, *Phys. Rev. B* **67**, 094432 (2003).
- ²⁷ S. Jekal, S. H. Rhim, S. C. Hong, W.-j. Son, and A. B. Shick, *Phys. Rev. B* **92**, 064410 (2015).
- ²⁸ D.-S. Wang, R. Wu, and A. J. Freeman, *Phys. Rev. B* **47**, 14932 (1993).